Pharmaceutical Sciences and Drug Design
ISSN: 3062-4428
2025, Volume 5, Page No: 283-296

Available online at: www.galaxypub.co/page/journals

Galaxy Publication

Design, Biological Evaluation, and PPARγ Modulation of Nitro- and Acetamidophenoxyisobutyric Acids as Antidiabetic Agents

Kenji Nakamura[1]*, Aiko Fujita[1]

[1]Department of Pharmaceutical Innovation, Faculty of Pharmaceutical Sciences, Osaka University, Osaka, Japan.

***E-mail** ✉ kenji.nakamura@outlook.com

Received: 24 November 2024; **Revised:** 14 February 2025; **Accepted:** 18 February 2025

ABSTRACT

Four isobutyric acid derivatives, including two nitro- and two acetamido-substituted analogues, were synthesized through a two-step procedure and fully characterized by spectroscopic techniques. Treatment of 3T3-L1 adipocytes with compounds 1–4 resulted in elevated mRNA expression levels of PPARγ and GLUT-4, two well-established molecular targets in diabetes therapy, whereas no detectable induction of PPARα expression was observed in vitro. Computational docking and molecular dynamics simulations supported favorable binding interactions between the synthesized molecules and PPARγ. In vivo evaluations demonstrated that all tested compounds exerted antihyperglycemic effects linked to enhanced insulin sensitivity. Among the series, nitrocompound 2 exhibited the most pronounced activity and oral bioavailability. Its mechanism of action may involve selective modulation of PPARγ, potentially facilitated by an additional stabilizing interaction with the Gln-286 residue. Overall, these findings identify nitrocompound 2 as a promising experimental candidate for antidiabetic drug development.

Keywords: Molecular dynamics, Drug design, PPAR, Diabetes

How to Cite This Article: Nakamura N, Fujita A. Design, Biological Evaluation, and PPARγ Modulation of Nitro- and Acetamidophenoxyisobutyric Acids as Antidiabetic Agents. Pharm Sci Drug Des. 2025;5:283-96. https://doi.org/10.51847/NlNkX8Fh31

Introduction

Phenoxyisobutyric acid–based compounds constitute the fibrate family of lipid-lowering agents and are primarily recognized for their ability to modulate peroxisome proliferator-activated receptors (PPARs) [1]. The α and γ isoforms of PPARs interact with endogenous fatty acids and are centrally involved in lipid homeostasis as well as the regulation of insulin sensitivity [2]. Among their downstream effects, PPARγ plays a critical role in controlling genes associated with glucose utilization, including the facilitative glucose transporter GLUT-4 [3]. Clofibrate, the earliest fibrate introduced into clinical practice, is administered as an ester prodrug that is enzymatically hydrolyzed in vivo to produce clofibric acid, the pharmacologically active form responsible for its lipid-lowering properties [4]. Beyond its hypolipidemic action, emerging evidence indicates that clofibrate and its metabolite significantly suppress the activity of 11β-hydroxysteroid dehydrogenase type 1 [5]. This enzyme mediates the regeneration of cortisol from cortisone elevated cortisol levels antagonize insulin signaling and enhance hepatic glucose production, ultimately contributing to hyperglycemia [6]. Type 2 diabetes mellitus is therefore characterized by persistent elevations in blood glucose resulting from defects in insulin secretion, insulin action, or both [7]. Within the framework of our ongoing efforts to identify novel antidiabetic agents, the present work reports the synthesis of four isobutyric acid derivatives (1–4), **(Figure 1),** their effects on PPARα/γ activation and GLUT-4 gene expression in vitro, computational simulations aimed at predicting their pharmacodynamic behavior, and an evaluation of their antidiabetic efficacy in a diabetic mouse model. The combined application of experimental and computational approaches exemplifies an integrated screening strategy for antidiabetic drug discovery [5].

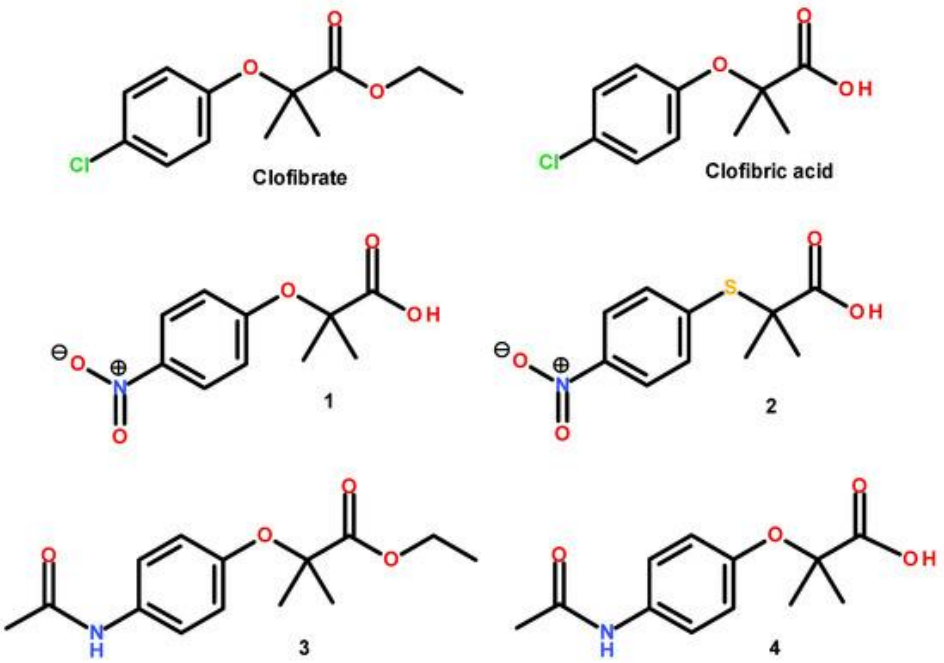

Figure 1. Chemical structures of the PPARα ligands clofibrate and clofibric acid, both featuring the phenoxyisobutyric acid core, together with the newly designed nitro derivatives (1–2) and acetamide derivatives (3–4).

Materials and Methods

Chemical methods

All starting materials and reagents were sourced from Merck® (Darmstadt, Germany) and utilized without further purification. Proton and carbon nuclear magnetic resonance spectra were acquired using a Varian Oxford spectrometer (Palo Alto, CA, USA) operating at 600 MHz for ^1H and 150 MHz for ^13C. Molecular weight analysis was carried out on a JMS-700 mass spectrometer (JEOL, Tokyo, Japan) using electron impact ionization. Melting points were determined with an EZ-Melt MPA120 automated melting point apparatus (Stanford Research Systems, Sunnyvale, CA, USA).

Synthesis of Compounds 1–4

2-(4-nitrophenoxy)isobutyric acid (1)

4-Nitrophenol (1.0 g, 4.44 mmol) was dissolved in acetonitrile together with potassium carbonate (1.22 g, 8.88 mmol). Ethyl 2-bromo-2-methylpropionate (1.29 g, 6.66 mmol) was added slowly, and the reaction mixture was refluxed for 8 h. After cooling, the mixture was poured into ice-cold water, yielding an oily intermediate. This material was subjected to alkaline hydrolysis using LiOH (5 equiv.) in a THF/MeOH/H_2O mixture (3:2:1, v/v/v) at ambient temperature for 3 h. Following acidification with 10% HCl and solvent removal, the crude product was extracted with dichloromethane. Drying, filtration, and concentration afforded a yellow solid, which was purified by recrystallization from chloroform to give compound 1 (62.8% yield m.p. 122.8–124.3 °C) [8, 9] yield 62.8%. ^{1}H NMR (200 MHz, $CDCl_3$) δ:1.71 (s, 6H, $(CH_3)_2$), 6.91 (d, 2H, H-2′, H-6′, J = 9.2 Hz), 8.16 (d, 2H, H-3′, H-5′, J = 9.6), 10.60 (s, 1H, CO_2H) ppm. ^{13}C NMR (50 MHz, CDCl3) δ: 25.5 ($(CH_3)_2$), 79.8 (C-2), 118.2 (C-2′, C-6′), 125.7 (C-3′, C-5′), 142.3 (C-4′), 160.6 (C-1′), 179.1 (COOH) ppm. MS/EI: m/z (% rel. int.). 225 (M^+, 1%), 180 (M-45, 100%). Anal. calcd. for $C_{10}H_{11}NO_5$: C, 53.33 H, 4.92 N, 6.22. Found: C, 53.41 H, 4.83 N, 6.28.

2-(4-nitrophenylsulfanyl)isobutyric acid (2)

A suspension of 4-nitrothiophenol (1.0 g, 6.40 mmol) and potassium carbonate (1.94 g, 14.1 mmol) in acetonitrile was treated dropwise with ethyl 2-bromoisobutyrate (1.37 g, 7.04 mmol) and heated under reflux for 6 h. Upon completion, the reaction mixture was quenched with cold water. The resulting crude material was hydrolyzed with

LiOH (5 equiv.) in THF/MeOH/H_2O (3:2:1, v/v/v) for 3 h at room temperature. Acidification and extraction with dichloromethane yielded a yellow solid, which was recrystallized from chloroform to afford compound 2 in 58.9% yield with a melting point of 121.9–123.7 °C [10, 11] yield 58.9%. ^{1}H NMR (400 MHz, $CDCl_3$) δ: 1.56 (s, 6H, $(CH_3)_2$), 7.65 (dd, 2H, H-2′, H-6′, J = 2.6, J = 9.6 Hz), 8.17 (dd, 2H, H-3′, H-5′, J = 2.6, J = 9.6 Hz), 10.60 (s, 1H, CO_2H) ppm. ^{13}C NMR (100 MHz, $CDCl_3$) δ: 25.9 ($(CH_3)_2$), 51.5 (C-2), 123.8 (C-2′, C-6′), 136.1 (C-3′, C-5′), 140.6 (C-1′), 145.4 (C-4′), 179.9 (COOH) ppm. MS/EI: m/z (% rel. int.). 241 (M^+, 1%), 196 (M-45, 100%). Anal. calcd. for $C_{10}H_{11}NO_4S$: C, 49.78 H, 4.60 N, 5.81 S, 13.29. Found: C, 49.69 H, 4.60 N, 5.87 S, 13.36.

Ethyl 2-[4-(acetylamino) phenoxy]isobutyrate (3)

4-Acetylaminophenol (1.0 g, 6.6 mmol) and potassium carbonate (2.0 g, 14 mmol) were dissolved in dimethyl sulfoxide and preheated at 40 °C. Ethyl 2-bromo-2-methylpropionate (1.45 mL, 9.9 mmol) was then introduced dropwise, and the reaction mixture was heated to reflux (80 °C) for 15 h. Reaction progress was monitored by TLC. After completion, the mixture was filtered, and the solid product was recrystallized from acetone to yield compound 3 as white crystals (44.0% yield m.p. 90.1–92.3 °C) [12]. yield 44.0%. ^{1}H NMR (200 MHz DMSO-d_6 Me_4Si) δ: 1.17 (3H, t, CH_3), 1.47 (6H, s, $(CH_3)_2$), 2.00 (3H, s, CH_3CO), 4.15 (2H, q, CH_2), 6.75 (2H, d, H-2′, H-6′, J = 8.7 Hz), 7.45 (2H, d, H-3′, H-5′, J = 8.7 Hz), 9.83 (1H, bs, N–H) ppm. ^{13}C NMR (50 MHz, DMSO-d_6) δ: 14.6 (CH_3), 24.5 (CH_3CO), 25.7 ($(CH_3)_2$), 61.6 (C-2), 79.5 (CH_2-O), 120.3 (C-2′, C-6′), 120.7 (C-3′, C-5′), 134.7 (C-4′), 150.9 (C-1′), 168.4 (NHC=O), 173.7 (O-C=O) ppm. EI-MS: m/z (rel. int.) 265 (M^+, 25%), 192 (25%), 151 (50%), 109 (100%). Anal. calcd. for $C_{14}H_{19}NO_4$: C, 63.38 H, 7.22 N, 5.28. Found: C, 63.38 H, 7.07 N, 5.53.

2-(4-nitrophenylsulfanyl)isobutyric acid (2)

Compound 2 was synthesized by reacting 4-nitrothiophenol (1.0 g, 6.40 mmol) with potassium carbonate (1.94 g, 14.1 mmol) in acetonitrile, followed by the gradual addition of ethyl 2-bromoisobutyrate (1.37 g, 7.04 mmol). The reaction mixture was maintained under reflux conditions for 6 h with continuous stirring. After completion, the mixture was quenched by pouring into chilled water, yielding an oily intermediate.

This crude product was immediately subjected to alkaline hydrolysis using lithium hydroxide (5 equivalents) in a ternary solvent system composed of THF, methanol, and water (3:2:1, v/v/v) and stirred at ambient temperature for 3 h. Subsequent acidification with aqueous hydrochloric acid (10% v/v) and partial solvent evaporation afforded a solid residue. Extraction with dichloromethane (3 × 10 mL), followed by drying over anhydrous sodium sulfate, filtration, and concentration, produced a yellow solid. Recrystallization from chloroform yielded compound 2 as a pure material (58.9% yield), with a melting point of 121.9–123.7 °C [10, 11] yield 58.9%. ^{1}H NMR (400 MHz, $CDCl_3$) δ: 1.56 (s, 6H, $(CH_3)_2$), 7.65 (dd, 2H, H-2′, H-6′, J = 2.6, J = 9.6 Hz), 8.17 (dd, 2H, H-3′, H-5′, J = 2.6, J = 9.6 Hz), 10.60 (s, 1H, CO_2H) ppm. ^{13}C NMR (100 MHz, $CDCl_3$) δ: 25.9 ($(CH_3)_2$), 51.5 (C-2), 123.8 (C-2′, C-6′), 136.1 (C-3′, C-5′), 140.6 (C-1′), 145.4 (C-4′), 179.9 (COOH) ppm. MS/EI: m/z (% rel. int.). 241 (M^+, 1%), 196 (M-45, 100%). Anal. calcd. for $C_{10}H_{11}NO_4S$: C, 49.78 H, 4.60 N, 5.81 S, 13.29. Found: C, 49.69 H, 4.60 N, 5.87 S, 13.36.

Ethyl 2-[4-(acetylamino)phenoxy]isobutyrate (3)

For the preparation of compound 3, 4-acetylaminophenol (1.0 g, 6.6 mmol) and potassium carbonate (2.0 g, 14 mmol) were dissolved in the minimum required volume of dimethyl sulfoxide and warmed to 40 °C. After 20 min of equilibration, ethyl 2-bromo-2-methylpropionate (1.45 mL, 9.9 mmol) was added slowly. The reaction mixture was then heated under reflux at 80 °C and monitored by TLC until completion (15 h).

Upon cooling, the mixture was filtered, and the crude solid was purified by recrystallization from acetone, affording compound 3 as white crystalline material (44.0% yield m.p. 90.1–92.3 °C) [12] yield 44.0%. ^{1}H NMR (200 MHz DMSO-d_6 Me_4Si) δ: 1.17 (3H, t, CH_3), 1.47 (6H, s, $(CH_3)_2$), 2.00 (3H, s, CH_3CO), 4.15 (2H, q, CH_2), 6.75 (2H, d, H-2′, H-6′, J = 8.7 Hz), 7.45 (2H, d, H-3′, H-5′, J = 8.7 Hz), 9.83 (1H, bs, N–H) ppm. ^{13}C NMR (50 MHz, DMSO-d_6) δ: 14.6 (CH_3), 24.5 (CH_3CO), 25.7 ($(CH_3)_2$), 61.6 (C-2), 79.5 (CH_2-O), 120.3 (C-2′, C-6′), 120.7 (C-3′, C-5′), 134.7 (C-4′), 150.9 (C-1′), 168.4 (NHC=O), 173.7 (O-C=O) ppm. EI-MS: m/z (rel. int.) 265 (M^+, 25%), 192 (25%), 151 (50%), 109 (100%). Anal. calcd. for $C_{14}H_{19}NO_4$: C, 63.38 H, 7.22 N, 5.28. Found: C, 63.38 H, 7.07 N, 5.53.

2-(4-acetamidophenoxy)isobutyric acid (4)

Compound 4 was obtained through selective ester hydrolysis of compound 3 (0.5 g, 1.88 mmol). The reaction was carried out in a THF/H_2O mixture (5:1, v/v) with lithium hydroxide (3 equivalents) at room temperature for 3 h. Following completion, the mixture was acidified with aqueous HCl (10% v/v), and organic solvents were removed under reduced pressure.

The remaining solid was extracted with dichloromethane (3 × 10 mL), dried over sodium sulfate, filtered, and concentrated. Recrystallization from methanol afforded compound 4 as a white solid in high yield (83.13%), with a melting point of 164.4–166.3 °C [13] yield 83.13%. ^{1}H NMR (200 MHz DMSO-d_6 Me_4Si) δ 1.46 (6H, s, $(CH_3)_2$), 2.10 (3H, s, CH_3CO), 6.78 (2H, d, H-2′, H-6′, J = 8.7 Hz), 7.44 (2H, d, H-3′, H-5′, J = 8.7 Hz), 9.83 (2H, bs, N–H, COOH) ppm. ^{13}C NMR (50 MHz, DMSO-d_6) δ: 23.8 (CH_3CO), 25.1 ($(CH_3)_2$), 78.7 (C-2), 119.5 (C-2′, C-6′), 120.2 (C-3′, C-5′), 133.9 (C-4′), 161.8 (C-1′), 167.9 (NHC=O), 175.2 (COOH) ppm. EI-MS: m/z (rel. int.) 237 (M^+, 5%), 192 (M-45, 100%). Anal. calcd. for $C_{12}H_{15}NO_4$: C, 60.75 H, 6.37 N, 5.90. Found: C, 60.8 H, 6.39 N, 5.85.

Biological evaluation

Quantification of GLUT-4 and PPAR expression

3T3-L1 fibroblasts were cultured to confluence and differentiated into adipocytes using dexamethasone acetate (0.25 μM), 3-isobutyl-1-methylxanthine (0.5 mM), and bovine insulin (0.8 μM). After 10 days, mature adipocytes were exposed for 24 h to cumulative concentrations of compounds 1–4.

Total RNA was isolated, and 2 μg of RNA was reverse-transcribed to cDNA. Quantitative PCR was performed using SYBR Green Master Mix with gene-specific primers for GLUT-4 (NM009204.2), PPARγ (NM011146.1), and PPARα (NM011144). Expression levels were normalized against the housekeeping gene 36B4 (NM007475.2). Relative gene expression changes were calculated using the ΔΔCt method and graphically represented [14, 15].

In vivo antidiabetic evaluation

Experimental animals

Male ICR mice (25 ± 5 g) were housed under controlled conditions (25 °C, 12 h light/dark cycle) with free access to food and water. All experimental procedures complied with Mexican regulations NOM-065-ZOO-1999 and NOM-033-ZOO-2014 and were approved by the Institutional Ethics Committee of the Universidad Autónoma Metropolitana (dictum 1857), in accordance with NIH guidelines.

Acute antidiabetic model

Diabetes was induced following previously reported protocols [5, 14]. After an 8 h fast, mice received nicotinamide (20 mg/kg, i.p.), followed 15 min later by streptozotocin (100 mg/kg, i.p.) dissolved in citrate buffer (0.05 M, pH 4.5). Animals exhibiting fasting glucose levels above 180 mg/dL were selected.

After a further fasting period, mice (n = 6 per group) were orally administered compounds 1–4 (100 mg/kg), vehicle (10% Tween 80), or reference drugs (glibenclamide, 20 mg/kg pioglitazone, 30 mg/kg). Blood glucose levels were recorded at baseline and at 1, 3, 5, and 7 h post-administration using a glucometer.

Molecular docking studies

Docking simulations were conducted using AutoDock Vina [16]. The crystal structure of PPARγ complexed with EHA (PDB ID: 2F4B, resolution 2.07 Å) was retrieved from the Protein Data Bank. Water molecules were removed, hydrogen atoms added, and Gasteiger charges assigned using MGLTools 1.5.4 [17]. Ligand structures were generated, minimized, and ionized using MOE with the MMFF94 force field [18].

The docking grid was centered on the co-crystallized ligand coordinates (8.693, −6.961, 39.672) with dimensions of 40 × 40 × 40 points and 0.375 Å spacing. One hundred genetic algorithm runs were performed, and poses were clustered using a 2.0 Å RMSD cutoff. Visualization and interaction analyses were carried out using MOE and PyMol.

Docking validation

Method validation was achieved by redocking EHA into the PPARγ binding site. The resulting RMSD value of 0.53 Å confirmed accurate reproduction of the crystallographic binding mode.

Molecular dynamics simulations

Ligand–protein complexes involving compounds 1–4, clofibric acid, pioglitazone, and EHA bound to PPARγ (PDB ID: 2F4B) were subjected to molecular dynamics simulations. These simulations aimed to assess the stability, conformational behavior, and interaction persistence of the complexes, following a previously established protocol [19].

Statistical analysis

Comparisons of glycemic variation percentages, as well as in vitro measurements of PPARγ and GLUT-4 expression, were evaluated using one-way analysis of variance (ANOVA) followed by Dunnett's post hoc multiple comparison test. Experimental data are reported as mean values ± standard error of the mean (SEM). A probability value of $p < 0.05$ was considered statistically significant. All statistical analyses were carried out using GraphPad Prism software (version 5.0).

Results and Discussion

Chemistry

The synthetic route leading to compounds 1 and 2 is outlined in **Figure 2.** These molecules were obtained through a nucleophilic substitution reaction in which ethyl 2-bromo-2-methylpropionate (7) reacted with either 4-nitrophenol (5) or 4-nitrothiophenol (6). The reactions were carried out under basic conditions using acetonitrile as the reaction medium, yielding the corresponding ethyl ester intermediates as oily residues. Without further purification, these ester intermediates were subjected to hydrolysis using lithium hydroxide (five equivalents) in a mixed solvent system consisting of THF, methanol, and water (3:2:1), resulting in the formation of compounds 1 and 2 with moderate isolated yields of 62.8% and 58.9%, respectively.

Compound 3 was synthesized following an analogous procedure, in which 4-acetylaminophenol served as the nucleophilic reagent. In this case, dimethyl sulfoxide was employed as the solvent under basic conditions, affording compound 3 as a white solid in 44% yield. Subsequent selective cleavage of the ester group using lithium hydroxide produced compound 4 in a significantly higher yield of 83.13% **(Figure 2).**

Reaction progress was routinely monitored by thin-layer chromatography (TLC). Final products were isolated either by filtration or by extraction with dichloromethane (CH_2Cl_2), providing compounds 1–4 in overall yields ranging from 44% to 83%. Purification was achieved by recrystallization using appropriate solvents, as detailed in materials and methods section. Structural confirmation of all synthesized compounds was accomplished through spectroscopic techniques, including ^{1}H and ^{13}C NMR, as well as mass spectrometric analysis. Elemental microanalysis was performed to verify compound purity.

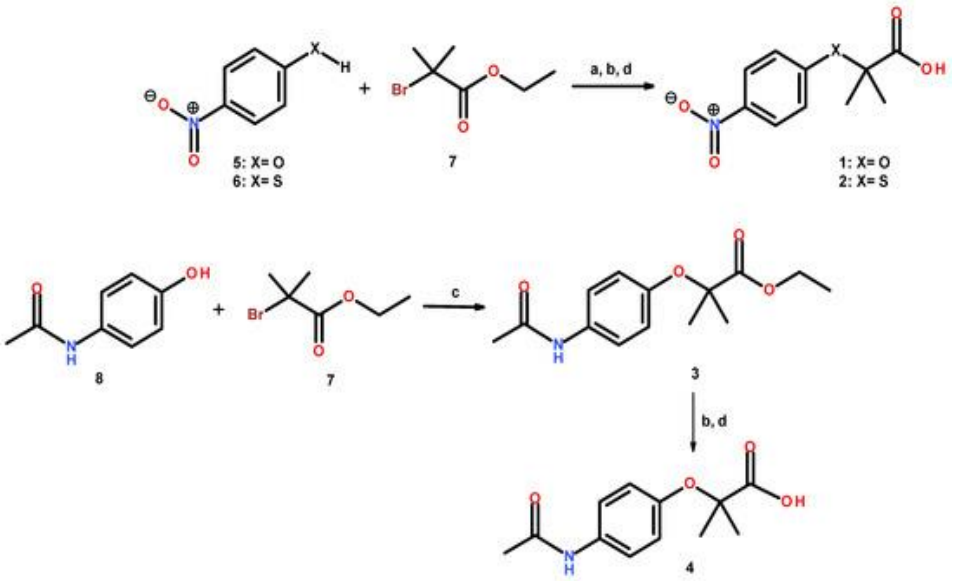

Figure 2. Synthetic pathway for compounds 1–4. Reaction conditions: (a) K_2CO_3 in CH_3CN under reflux (b) hydrolysis with LiOH in THF/MeOH/H_2O (c) K_2CO_3 in DMSO at 80 °C (d) acidic workup with 10% (v/v) HCl.

In the ^{1}H NMR spectra, proton resonances were systematically assigned on the basis of their chemical shifts, signal multiplicities, and coupling constants (J values). All synthesized compounds exhibited a single resonance in the region of δ_H 1.46–1.71 ppm, corresponding to the geminal dimethyl moiety. Signals characteristic of para-disubstituted aromatic rings were observed in every molecule. Specifically, the aromatic region displayed a typical A_2B_2 spin system, with doublets appearing between δ_H 6.75–7.65 ppm (J_ortho = 8.7–9.6 Hz) and 7.45–8.17 ppm (J_ortho = 8.4–9.6 Hz), which were assigned to the equivalent H-2′/H-6′ and H-3′/H-5′ protons, respectively. For compounds 1, 2, and 4, the acidic proton of the carboxyl group appeared as a singlet in the range of δ_H 9.83–10.6 ppm. In addition, compounds 3 and 4 showed a singlet attributable to the acetamide methyl protons at δ_H 2.0–2.1 ppm.

Analysis of the ^{13}C NMR spectra revealed consistent resonance patterns across all compounds. A signal between δ_C 24.5 and 25.7 ppm was assigned to the geminal dimethyl carbons, while an additional resonance between δ_C 51.5 and 79.8 ppm corresponded to the C-2 carbon of the ether linkage. In the aromatic carbon region, resonances at δ_C 118.2–120.3 ppm and 120.2–136.1 ppm were attributed to C-2′/C-6′ and C-3′/C-5′, respectively. Further downfield signals were observed between δ_C 133.7–145.4 ppm for C-4′, 140.6–161.8 ppm for C-1′, and 175.2–179.9 ppm for the carboxylic acid carbonyl carbon. For compounds 3 and 4, additional resonances associated with the acetamide group (CH_3CONH–) were detected, including methyl carbon signals at δ_C 23.8–24.5 ppm and carbonyl carbon signals at δ_C 167.9–168.4 ppm.

In vitro PPARα/γ and GLUT-4 expression

Prior to gene expression analysis, the cytotoxic potential of compounds 1–4 was assessed in 3T3-L1 fibroblasts using the MTT assay at concentrations of 1, 10, and 100 μM. No reduction in cell viability was detected at any tested concentration. To evaluate the effects of the synthesized compounds on gene expression, murine fibroblasts were induced to differentiate into adipocytes, enabling the assessment of PPARα, PPARγ, and GLUT-4 mRNA levels. Differentiated cells were exposed to compounds 1–4 at a concentration of 10 μM for 24 h. Pioglitazone (PIO) and clofibrate (CLO) served as reference agonists and were included as positive controls [14, 15].

Quantitative real-time PCR (qPCR) was employed to determine changes in mRNA expression. As illustrated in **Figure 3**, treatment with compounds 1–4 led to a statistically significant increase in PPARγ transcript levels, with an approximate two- to four-fold elevation, accompanied by a three-fold upregulation of its downstream target gene GLUT-4, comparable to the response observed with pioglitazone (PIO). Activation of PPARγ is known to lower blood glucose levels in diabetic patients by improving insulin sensitivity, while increased GLUT-4 expression in skeletal muscle is essential for maintaining glucose balance. Notably, the findings of this study indicate that nitro derivatives 1 and 2, as well as acetamide compound 4, enhanced GLUT-4 mRNA expression to a greater extent than pioglitazone, as shown in **Figure 3b.**

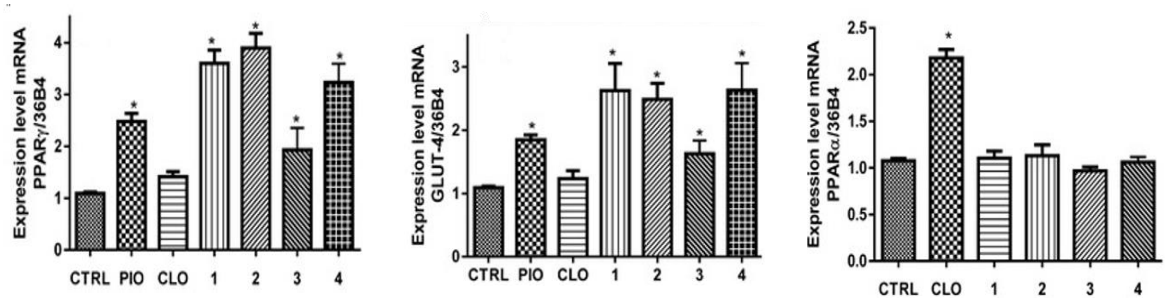

a) b) c)

Figure 3. Modulation of gene expression levels of PPARγ (a), GLUT-4 (b), and PPARα (c) following treatment with pioglitazone, clofibrate, and isobutyric acid derivatives 1–4. * Statistically significant differences between treated groups and the control were determined by one-way ANOVA followed by Dunnett's post hoc test (n = 5, values expressed as mean ± SEM, $p < 0.001$ versus CTRL).

As anticipated, clofibrate (CLO) failed to induce a significant increase in PPARγ or GLUT-4 mRNA expression. In contrast, none of the synthesized derivatives produced measurable changes in PPARα transcript levels, whereas clofibrate retained its known activity toward this receptor. These findings indicate that replacement of the chlorine atom on the aromatic ring with aza-containing substituents, such as nitro or acetamide groups, confers preferential

activation of PPARγ over PPARα. Consequently, the synthesized molecules can be classified as selective PPAR modulators (SPPARMs) [20].

In vivo antidiabetic activity

To validate the hypoglycemic and/or antihyperglycemic potential of compounds 1–4, an acute in vivo study was conducted using a mouse model of diabetes induced by streptozotocin (STZ) in combination with nicotinamide (NA). Glibenclamide (Gli) was included as a hypoglycemic reference to confirm partial pancreatic β-cell impairment and to ensure preserved insulin secretion and responsiveness to insulin secretagogues. Pioglitazone was employed as a positive control for antihyperglycemic activity mediated through PPARγ activation. The outcomes of this study are summarized in **Figure 4**.

Oral administration of compounds 1, 2, and 4 at a dose of 100 mg/kg via the intragastric route resulted in a pronounced reduction in blood glucose levels within 60 minutes compared to the vehicle-treated group (Tween 80, 10%). This glucose-lowering effect persisted throughout the duration of the experiment. Notably, blood glucose concentrations did not decrease below physiological baseline values, in contrast to the response observed with glibenclamide. This profile indicates an antihyperglycemic mechanism consistent with enhanced insulin sensitivity driven by PPARγ activation [21], as evidenced by the similar glycemic response observed with pioglitazone. Compound 3, however, exhibited a delayed glucose-lowering effect, becoming evident only at 5 and 7 hours after administration. This delayed onset suggests that compound 3 may function as a prodrug of compound 4, requiring metabolic activation through phase I hydrolytic processes in vivo.

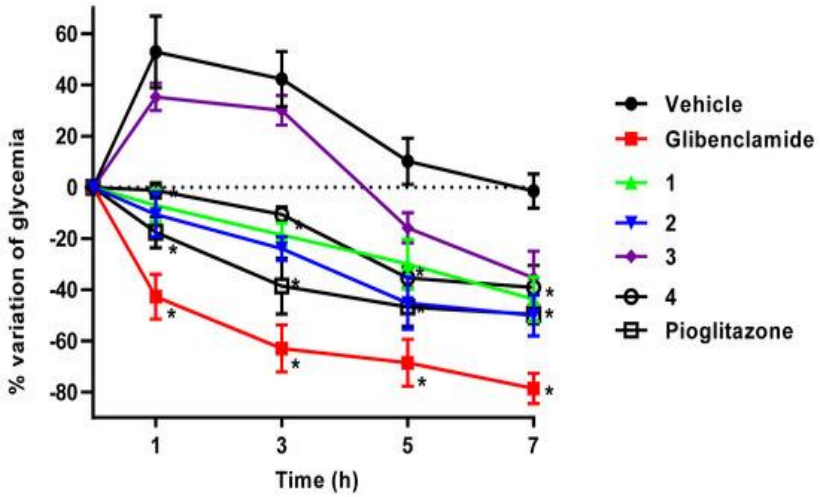

Figure 4. Blood glucose response in STZ/NA-induced diabetic mice following a single intragastric dose (100 mg/kg) of (thio)phenoxyisobutyric acid derivatives 1–4, glibenclamide, or pioglitazone. * Statistical significance versus the control group was determined using one-way ANOVA with Dunnett's multiple comparison test (n = 6, mean ± SEM, $p < 0.05$).

Molecular docking analysis

Based on the observed biological effects, including stimulation of PPARγ and GLUT-4 expression in vitro and reduction of hyperglycemia in vivo, compounds 1–4 were further evaluated using structure-based computational methods. Docking simulations revealed that these derivatives are favorably positioned within the ligand-binding cavity of PPARγ (PDB ID: 2F4B). The predicted binding modes indicated the establishment of a hydrogen-bonding interaction with His-323, accompanied by several stabilizing polar contacts involving Cys-285, Tyr-327, Tyr-473, and His-449, residues that are critically associated with receptor activation **(Figures 5 and 6)**. A comparable interaction profile has previously been documented for (5-{3-[(6-benzoyl-1-propyl-2-naphthyl)oxy]propoxy}-1H-indol-1-yl)acetic acid (EHA), a ligand crystallographically resolved in complex with PPARγ, which engages overlapping amino acid residues within the binding site [22]. In contrast, compound 3 failed to establish key receptor interactions, a result that aligns with its comparatively weak biological responses observed in both cellular and animal studies. Of particular note, nitro-bearing compounds 1 and 2 contributed additional polar interactions, specifically involving His-449, His-323, and Ser-289, which may underlie their enhanced activity. Clofibric acid was included as a reference ligand and docked into the same receptor site.

Relative to compounds 1–4, clofibric acid displayed reduced predicted binding strength toward PPARγ. Validation of the docking protocol yielded a root-mean-square deviation (RMSD) of 0.53 Å², indicating reliable reproduction of ligand positioning. Visualization and analysis of protein–ligand interactions were conducted using PyMol and MOE software tools [18].

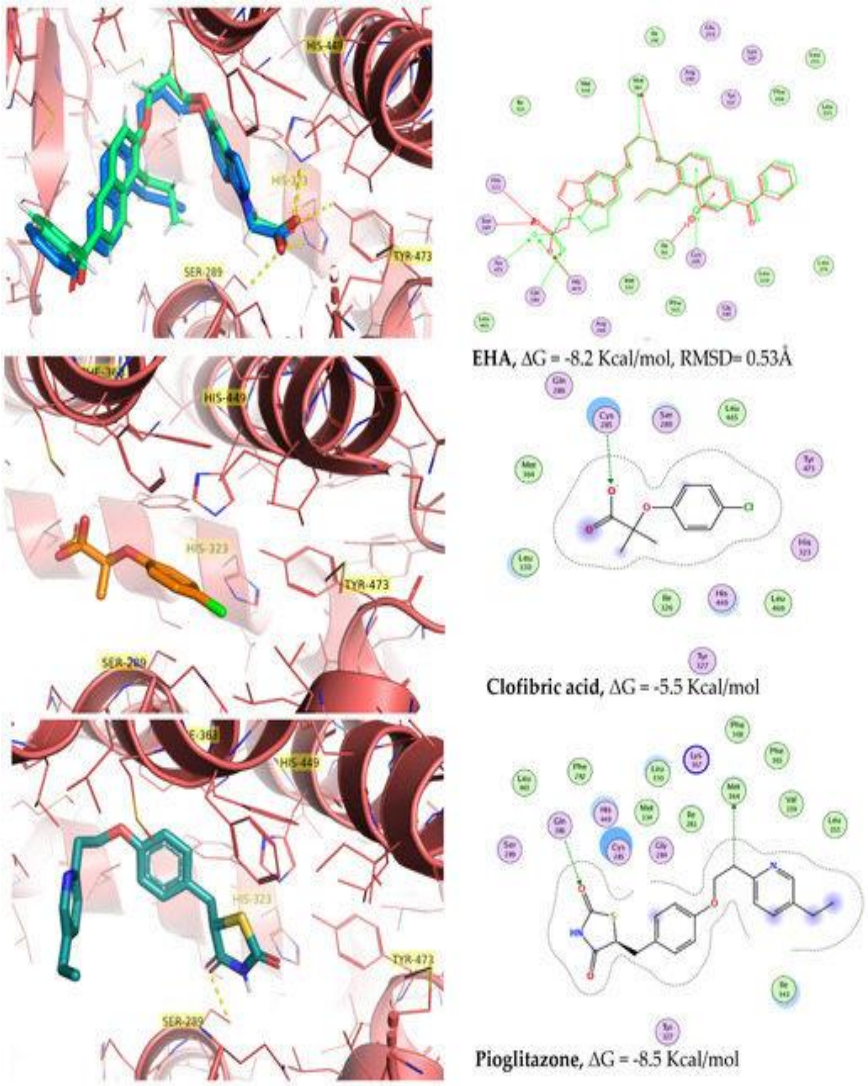

Figure 5. Three-dimensional binding conformations within the PPARγ ligand-binding domain (PDB ID: 2F4B). The reference ligand EHA is shown as the crystallographic structure (carbon atoms in blue) alongside its redocked conformation (carbon atoms in green). Predicted binding orientations of clofibric acid (carbon atoms in orange) and pioglitazone (carbon atoms in cyan) are also depicted, together with a two-dimensional representation of their key molecular interactions. For EHA, the two-dimensional superimposed interaction maps distinguish the experimental X-ray complex (green) from the redocked model (red).

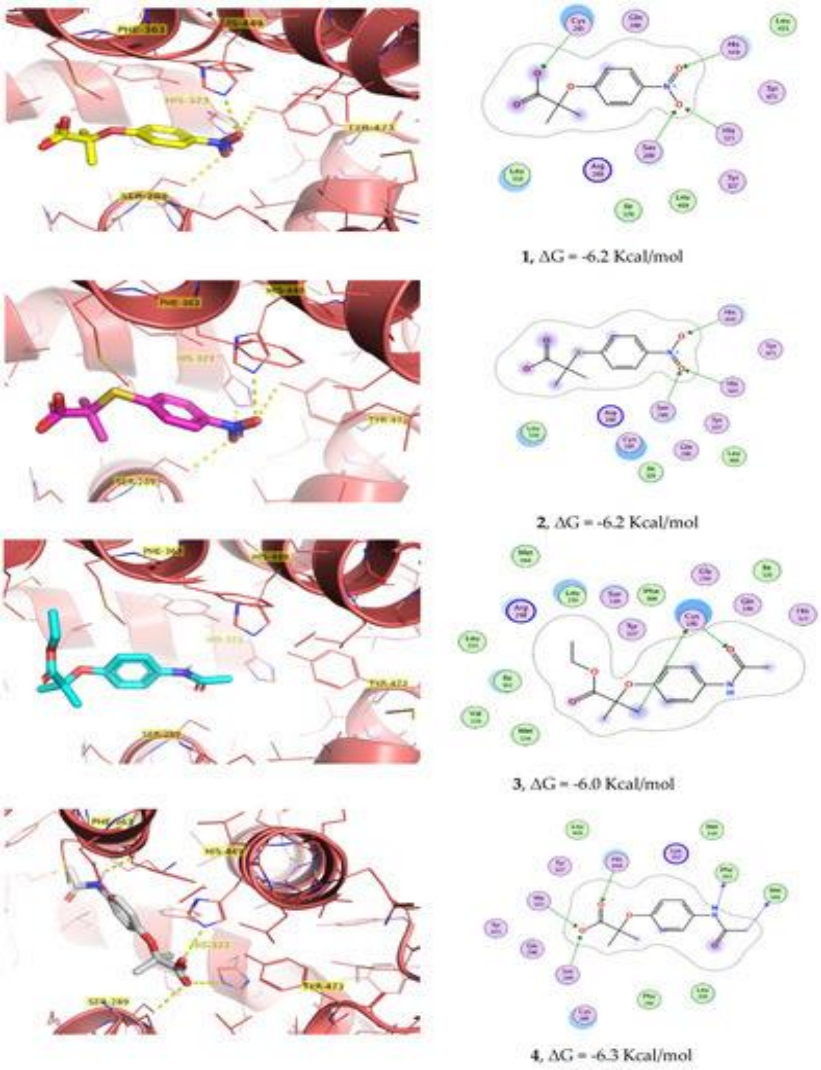

Figure 6. Predicted binding orientations of compounds 1–4 within the PPARγ ligand-binding pocket. Carbon atoms are shown in yellow for compound 1, magenta for compound 2, cyan for compound 3, and gray for compound 4. Corresponding two-dimensional interaction maps illustrating ligand–receptor contacts are also presented.

Compound 3, which retains its ethyl ester functionality, adopted a binding mode distinct from that of its hydrolyzed analogue 4, present in the ionized carboxylate form. While the aromatic ring of compound 3 was positioned to allow interactions with His-327 and Ser-289, the ester moiety was oriented toward a lateral sub-pocket of the PPARγ binding cavity **(Figure 6)**. The docking-derived binding energies and predicted inhibition constants (K_i) for compounds 1–4, together with those obtained for clofibrate, were consistent with the trends observed in both cellular and animal pharmacological evaluations **(Table 1).** These findings support the conclusion that the glucose-lowering activity of the tested compounds is primarily associated with enhanced insulin sensitivity.

Table 1. Docking scores, predicted binding affinities, molecular dynamics–derived binding energies, and quantitative pharmacological parameters for compounds 1–4, pioglitazone and clofibric acid.

Compound	Predicted Affinity Ki (μM)	PPARγ Docking Energy ΔG (kcal/mol)	PPARγ mRNA Induction (Fold Change)	PPARγ MD Binding Energy ΔG (kcal/mol)	GLUT-4 mRNA Induction (Fold Change)	Maximum Reduction in Blood Glucose (%)
1	5.39	−6.2	3.60	−7.3	2.62	−43.5
2	3.90	−6.2	3.89	−7.8	2.48	−50.1
3	7.54	−6.0	1.92	−7.2	1.62	−35.3

4	4.28	−6.3	3.23	−6.9	2.63	−39.1
Pioglitazone	0.50	−8.5	2.51	−9.7	1.84	−49.6
Clofibric acid	13.13	−5.5	1.41	−6.8	1.02	No significant effect observed [5]

Molecular dynamics simulations

Molecular dynamics (MD) simulations were performed to investigate the conformational behavior and stability of the protein–ligand complexes over time. The root-mean-square deviation (RMSD) profiles of both the PPARγ backbone and the bound ligands are presented in **Figure 7.** Among the analyzed systems, the complex containing nitrocompound 2 reached conformational stability shortly after 2 ns of simulation. Notably, the two most active complexes did not exceed RMSD values of 1.5 Å, indicating highly rigid binding modes. These systems maintained consistent RMSD values throughout the remainder of the simulation, reflecting stable protein–ligand interactions.

As shown, the RMSD trajectories of PPARγ in complex with compound 4 and clofibric acid exhibited comparable behavior between 8 and 20 ns. In contrast, the backbone RMSD patterns of the EHA- and pioglitazone-bound receptors reflected more pronounced conformational rearrangements, associated with cycles of protein folding and unfolding before reaching a quasi-equilibrium toward the end of the simulation. Analysis of ligand RMSD profiles revealed comparatively lower fluctuations, suggesting limited conformational variability once bound. In particular, compounds 1, 2, and 4 displayed RMSD oscillations centered around 1.5 Å after the first nanosecond, indicating rapid accommodation within the binding pocket and stable anchoring to neighboring amino acid residues previously identified through docking analysis. These observations further support the reliability of the docking predictions.

Inspection of **Figure 7** indicates that most compounds preserved key anchoring interactions with residues Lys-367, Tyr-327, and His-449. However, nitrocompound 2 exhibited an additional stabilizing interaction involving Gln-286. After approximately 2 ns of simulation, compound 2 established persistent contacts through its nitro group with Gln-286 and His-466, while its carboxylate moiety interacted with Lys-367 and Tyr-327 for the duration of the 20 ns simulation. Unlike the other derivatives, compound 2 induced a noticeable reorientation of the Gln-286 side chain. This residue is known to play a crucial role in stabilizing helices H3 and H12 of PPARγ, thereby exerting a significant influence on receptor activation [23].

Given that partial PPARγ modulators preferentially stabilize the β-sheet region and helix H3 to a greater extent than full agonists [24], nitrocompound 2 may be classified as a partial agonist, potentially offering a reduced side-effect profile. The enhanced stability observed during MD simulations, together with the unique interaction with Gln-286, is consistent with the strong biological activity of compound 2 observed in both in vitro and in vivo assays.

To further estimate the free binding energies of the PPARγ–ligand complexes, an additional computational approach was applied using the PRODIGY-LIG web server [25]. This platform employs a refinement-based strategy to calculate intermolecular interaction energies and is suitable for diverse protein–ligand systems. The analysis required only the three-dimensional structures of the complexes in PDB format. PRODIGY-LIG predicts binding affinities with a reported root-mean-square error (RMSE) of 1.89 kcal/mol. The resulting binding energy estimates are presented in **Table 1.** Calculations performed for the studied complexes yielded binding free energies comparable to those obtained from molecular docking, albeit slightly more negative, reflecting the stabilizing contribution of molecular dynamics refinement [26].

The design of PPAR-targeted therapeutics that retain efficacy while minimizing the adverse effects associated with full PPARγ agonists remains a central challenge in drug discovery. Consequently, the development of partial PPARγ agonists or selective PPARγ modulators (SPPARMs) represents a promising alternative strategy for the management of metabolic disorders. The compounds described in this study exemplify this approach and demonstrate favorable computational and pharmacological profiles.

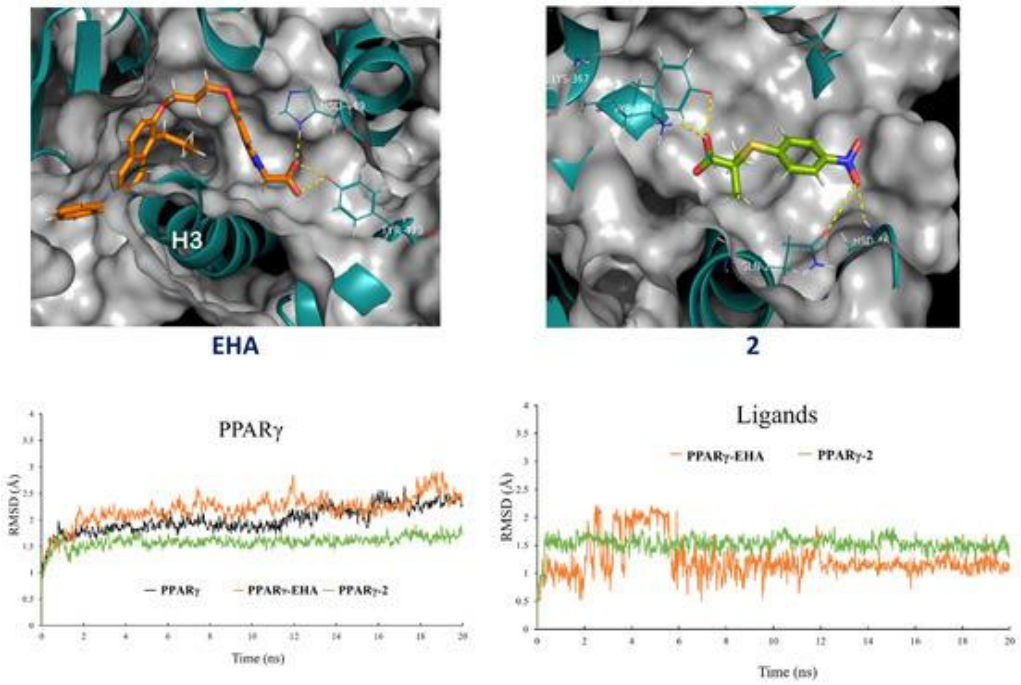

Figure 7. Comparison of hydrogen-bond interaction patterns formed by EHA (shown in orange) and nitrocompound 2 (shown in green) within the ligand-binding cavity of PPARγ (PDB ID: 2F4B), along with the corresponding RMSD trajectories of the receptor and bound ligands.

In silico toxicological evaluation

It is widely recognized that nitro-containing compounds are often associated with unpredictable and sometimes severe toxic responses, which has led to their classification as structural alerts and frequent exclusion from drug development pipelines [27]. Nonetheless, nitro functionalities may also serve a dual role, acting not only as pharmacophores but also as selective toxicophores that are linked to tissue-specific toxicity profiles [28]. In order to proactively assess potential safety concerns associated with compounds 1–4, a computational toxicological analysis was undertaken. Predicted toxicity parameters for compounds 1–4, as well as for clofibrate and pioglitazone, were generated using the ACD/ToxSuite software package (version 2.95), and the results are summarized in **Table 2.**

Table 2. In silico–estimated toxicity characteristics for compounds 1–4 in comparison with pioglitazone and clofibrate.

Compound	LD_{50} Mouse (mg/kg) p.o.	LD_{50} Mouse (mg/kg) i.p.	LD_{50} Rat (mg/kg) p.o.	LD_{50} Rat (mg/kg) i.p.	CYP1A2 Inhibition Probability	CYP3A4 Inhibition Probability	CYP2D6 Inhibition Probability	hERG Blockade Probability
1	1500	680	1590	820	0.00	0.00	0.00	0.01
2	790	670	1280	520	0.00	0.00	0.01	0.01
3	1900	810	3000	770	0.19	0.02	0.01	0.05
4	1400	790	2500	970	0.00	0.00	0.00	0.01
Pioglitazone	1400	400	1100	400	0.02	0.22	0.03	0.10
Clofibrate	1300	750	1800	1200	0.31	0.03	0.04	0.12

Computational predictions of cytochrome P450 inhibition indicated that compounds 1–4 display inhibition profiles for the three major CYP450 isoforms that are comparable to those of clofibrate at clinically relevant concentrations below 10 μM. These results suggest a minimal risk of drug–drug interactions and a low likelihood of adverse off-target effects. In addition, all four compounds showed a very low predicted tendency to block the hERG potassium channel at concentrations with Ki values below 10 μM, supporting their classification as non-cardiotoxic agents. Acute toxicity simulations further demonstrated that compounds 1–4 possess LD_{50} values similar to those predicted for clofibrate and pioglitazone when evaluated via two administration routes across two

murine models. Consistent with these in silico findings, experimental assessment of 3T3-L1 fibroblast viability confirmed the absence of cytotoxic effects for compounds 1–4 at concentrations up to 100 μM.

The concept of "toxicity cliffs" was first introduced by our group in 2015 [29] and subsequently revisited by other investigators in 2019 [30]. This term describes certain nitro-containing compounds that are flagged by in silico toxicity prediction tools as potentially mutagenic or carcinogenic—such as metronidazole, nimesulide, flutamide, and nitazoxanide—yet exhibit low toxicity in experimental settings. In the present study, compounds 1 and 2 can be classified within this category, as they demonstrate negligible toxic effects despite containing structural motifs commonly identified as toxicity alerts.

To further characterize the drug-likeness of compounds 1–4, their pharmacokinetic behavior was evaluated using the ADMETLab 2.0 platform [31]. Predicted ADME parameters are summarized in **Table 3** and include key absorption-related properties such as gastrointestinal uptake, blood–brain barrier penetration, and oral bioavailability.

Table 3. Predicted pharmacokinetic parameters generated using ADMETLab 2.0 (https://admetmesh.scbdd.com/, accessed 5 March 2021) for clofibrate and compounds 1–4.

ADME Category	Parameter	Clofibrate	1	2	3	4
Absorption	Gastrointestinal uptake	High (+)	High (+)	High (+)	High (+)	High (+)
	Predicted oral bioavailability (F)	> 30%	< 20%	> 30%	> 30%	> 30%
	Blood–brain barrier penetration	Yes (+)	No (−)	No (−)	Yes (+)	No (−)
Distribution	Plasma protein binding (%)	97.21	90.62	91.22	60.41	42.14
	Apparent volume of distribution (L/kg)	1.403	0.23	0.32	0.95	0.41
Metabolism	CYP3A4 substrate likelihood	Yes (++)	Yes (+)	Yes (+)	Yes (++)	Yes (+)
	CYP2D6 substrate likelihood	Yes (+)	No (−)	No (−)	Yes (+)	No (−)
Excretion	Total clearance (mL/min/kg)	5.202	0.948	0.412	5.860	1.093
	Predicted half-life (T½)	> 3 h	> 3 h	> 3 h	> 3 h	> 3 h

Compounds 1–4 were predicted to possess excellent oral absorption properties, whereas penetration of the blood–brain barrier was limited to compound 3 and the reference drug clofibrate. Drug distribution was evaluated using plasma protein binding and volume of distribution as key indicators. All compounds exhibited protein binding values below the commonly accepted threshold of 95%, suggesting favorable distribution profiles. Nonetheless, compounds with very high protein binding may suffer from a narrow therapeutic margin, as observed for clofibrate.

Predictions related to metabolic behavior indicated that compounds 1–4 are metabolized primarily by cytochrome P450 enzymes, highlighting this enzymatic family as the principal route of biotransformation, consistent with many small-molecule therapeutics. Elimination parameters further demonstrated that these compounds display adequate clearance rates and prolonged elimination half-lives exceeding 3 h, comparable to those calculated for clofibrate.

Conclusion

This study reports the successful synthesis of four 4-azasubstituted (thio)phenoxyisobutyric acid derivatives and demonstrates their pronounced biological activity. All compounds markedly enhanced the mRNA levels of PPARγ and its downstream target GLUT-4, exceeding the effects observed for the reference drugs clofibrate and pioglitazone. Notably, these derivatives exhibited selective modulation of PPARγ without activation of PPARα. Structurally, the compounds differ from clofibrate by the replacement of the para-chlorine atom on the aromatic ring with nitrogen-containing substituents, specifically nitro groups in compounds 1 and 2 and acetamide functionalities in compounds 3 and 4. In vivo evaluation revealed that compounds 1, 2, and 4 produced a significant antihyperglycemic response following oral administration in a diabetic animal model. This effect is consistent with an insulin-sensitizing mechanism and supports their classification as selective PPARγ modulators (SPPARMs), comparable to pioglitazone. Among the series, nitro-substituted compound 2 emerged as the most promising candidate. Molecular dynamics simulations highlighted its enhanced stability within the PPARγ ligand-

binding domain, attributed to additional interactions involving the nitro moiety and residue Gln-286. These features suggest that compound 2 may function as a partial PPARγ agonist, a profile associated with improved safety and reduced adverse effects.

Acknowledgments: None

Conflict of Interest: None

Financial Support: None

Ethics Statement: None

References

1. Giampietro L, Ammazzalorso A, Amoroso R, De Filippis B. Development of fibrates as important scaffolds in medicinal chemistry. ChemMedChem. 2019;14:1051-66.
2. Maltarollo VG, Kronenberger T, Windshugel B, Wrenger C, Trossini GHG, Honorio KM. Advances and challenges in drug design of PPARδ ligands. Curr Drug Targets. 2018;19:144-54.
3. Pujimulyani D, Yulianto WA, Setyowati A, Arumwardana S, Kusuma HSW, Sholihah IA, et al. Hypoglycemic activity of Curcuma mangga Val. extract via modulation of GLUT4 and PPAR-gamma mRNA expression in 3T3-L1 adipocytes. J Exp Pharmacol. 2020;8:363-9.
4. Thorp JM, Waring WS. Modification of metabolism and distribution of lipids by ethyl chlorophenoxyisobutyrate. Nature. 1962;194:948-9.
5. Navarrete-Vázquez G, Alaniz-Palacios A, Hidalgo-Figueroa S, González-Acevedo C, Ávila-Villarreal G, Estrada-Soto S, et al. Discovery, synthesis and in combo studies of a tetrazole analogue of clofibric acid as a potent hypoglycemic agent. Bioorg Med Chem Lett. 2013;23:3244-7.
6. Webster SP, Ward P, Binnie M, Craigie E, McConnell KMM, Sooy K, et al. Discovery and biological evaluation of adamantyl amide 11beta-HSD1 inhibitors. Bioorg Med Chem Lett. 2007;17:2838-43.
7. Álvarez-Almazán S, Filisola-Villaseñor JG, Alemán-González-Duhart D, Tamay-Cach F, Mendieta-Wejebe JE. Current molecular aspects in the development and treatment of diabetes. J Physiol Biochem. 2020;76:13-35.
8. Wang B, Tang C, Han Y, Guo R, Qian H, Huang W. Synthesis and preliminary antihyperlipidaemic activities evaluation of andrographolide derivatives. Med Chem. 2012;8:293-8.
9. Lalezari I, Rahbar S, Lalezari P, Fermi G, Perutz MF. LR16, a compound with potent effects on the oxygen affinity of hemoglobin, on blood cholesterol, and on low density lipoprotein. Proc Natl Acad Sci USA. 1988;85:6117-21.
10. Navarrete-Vázquez G, Villalobos-Molina R, Estrada-Soto S, Ortiz-Andrade R, Tlahuext H. 2-Methyl-2-(4-nitrophenylsulfanyl)propanoic acid. Acta Crystallogr Sect E Struct Rep Online. 2008;64:o91.
11. Andreani F, Andrisano R, Andreani A. New alpha-substituted arylthioacetic derivatives forming analogues of clofibrate. Farmaco Sci. 1975;30:847-58.
12. Navarrete-Vázquez G, Torres-Gómez H, Guerrero-Álvarez J, Tlahuext H. Synthesis and crystal structure of ethyl 2-[4-(acetylamino)phenoxy]-2-methylpropanoate. J Chem Crystallogr. 2011;41:732-6.
13. Navarrete-Vázquez G, Colín-Lozano B, Tlahuext H, Tapia-Benavides AR. 2-(4-Acetamidophenoxy)-2-methylpropanoic acid. Acta Crystallogr Sect E Struct Rep Online. 2013;9:o443.
14. Gutiérrez-Hernández A, Galván-Ciprés Y, Domínguez-Mendoza EA, Aguirre-Vidal Y, Estrada-Soto S, Almanza-Pérez JC, et al. Design, synthesis, antihyperglycemic studies, and docking simulations of benzimidazole-thiazolidinedione hybrids. J Chem. 2019;2019:1650145.
15. Giacoman-Martínez A, Alarcón-Aguilar FJ, Zamilpa A, Hidalgo-Figueroa S, Navarrete-Vázquez G, García-Macedo R, et al. Triterpenoids from Hibiscus sabdariffa L. with PPARδ/γ dual agonist action. Planta Med. 2019;85:412-23.
16. Trott O, Olson AJ. AutoDock Vina: Improving the speed and accuracy of docking with a new scoring function. J Comput Chem. 2010;31:455-61.
17. Jiang X, Kumar K, Hu X, Wallqvist A, Reifman J. DOVIS 2.0: An efficient and easy to use parallel virtual screening tool. Chem Cent J. 2008;2:18.

18. Molecular Operating Environment (MOE). Montreal (QC): Chemical Computing Group ULC; 2021. Available from: http://www.chemcomp.com
19. Hidalgo-Figueroa S, Rodríguez-Luévano A, Almanza-Pérez JC, Giacoman-Martínez A, Ortiz-Andrade R, León-Rivera I, et al. Synthesis, molecular docking, dynamic simulation and pharmacological characterization of potent multifunctional agent for type 2 diabetes. Eur J Pharmacol. 2021;907:174244.
20. Giampietro L, Laghezza A, Cerchia C, Florio R, Recinella L, Capone F, et al. Novel phenyldiazenyl fibrate analogues as PPAR α/γ/δ pan-agonists. ACS Med Chem Lett. 2019;10:545-51.
21. Sugii S, Olson P, Sears DD, Saberi M, Atkins AR, Barish GD, et al. PPARγ activation in adipocytes is sufficient for systemic insulin sensitization. Proc Natl Acad Sci USA. 2009;106:22504-9.
22. Mahindroo N, Wang CC, Liao CC, Huang CF, Lu IL, Lien TW, et al. Indol-1-yl acetic acids as peroxisome proliferator-activated receptor agonists. J Med Chem. 2006;49:1212-26.
23. Pochetti G, Godio C, Mitro N, Caruso D, Galmozzi A, Scurati S, et al. Insights into the mechanism of partial agonism. J Biol Chem. 2007;282:17314-24.
24. Bruning JB, Chalmers MJ, Prasad S, Busby SA, Kamenecka TM, He Y, et al. Partial agonists activate PPARgamma using a helix 12 independent mechanism. Structure. 2007;15:1258-71.
25. Vangone A, Schaarschmidt J, Koukos P, Geng C, Citro N, Trellet ME, et al. Large-scale prediction of binding affinity in protein-small ligand complexes. Bioinformatics. 2019;35:1585-7.
26. Kurkcuoglu Z, Koukos PI, Citro N, Trellet ME, Rodrigues JPGLM, Moreira IS, et al. Performance of HADDOCK and a simple contact-based predictor. J Comput Aided Mol Des. 2018;32:175-85.
27. Nepali K, Lee HY, Liou JP. Nitro-group-containing drugs. J Med Chem. 2019;62:2851-93.
28. Li JJ. Medicinal chemistry for practitioners. 1st ed. New York (NY): Wiley; 2020.
29. Medina-Franco JL, Navarrete-Vázquez G, Méndez-Lucio O. Activity and property landscape modeling. Future Med Chem. 2015;7:1197-211.
30. Alberga D, Trisciuzzi D, Mansouri K, Mangiatordi GF, Nicolotti O. Prediction of acute oral systemic toxicity using a multifingerprint similarity approach. Toxicol Sci. 2019;167:484-95.
31. Xiong G, Wu Z, Yi J, Fu L, Yang Z, Hsieh C, et al. ADMETlab 2.0: An integrated online platform for predictions of ADMET properties. Nucleic Acids Res. 2021;49:W5-14.